19th Brazilian Congress of Thermal Sciences and Engineering
November 6th–10th, 2022, Bento Gonçalves - RS - Brazil

ENC-2022-0075
AN INITIAL STUDY ON AN EV BATTERY PRISMATIC CELL THERMAL BEHAVIOR

Luciano Amaury dos Santos
Joaquim Manoel Gonçalves
Samuel Luna de Abreu
Andre Luiz Fuerback
Daniel Godoy Costa
Adriano de Andrade Bresolin
Instituto Federal de Santa Catarina, Av. Mauro Ramos, 950 – Centro -CEP 88020-300 – Florianópolis - SC
luciano.santos@ifsc.edu.br, joaquimm@ifsc.edu.br, abreu@ifsc.edu.br, andre.fuerback@ifsc.edu.br, danielgodoy@ifsc.edu.br, adriano.bresolin@ifsc.edu.br

Abstract. *Even dismissing its impact on global warming, air pollution due to IC engines in large cities is an important problem to which electrical vehicles (EVs) have been a very attractive solution. The relatively low thermodynamic efficiency of small IC engines when compared to the combination of big electric power plants and electrical motors also have pushed the engineers to the EV development at each Oil crisis. Historically the lack of adequate and accessible ways of storing electrical energy has made EV wide adoption unviable, but the fast advance in batteries technology over the last decades really created a new scenario, in which government regulations, along people enthusiasm, ensued a blossoming of EVs production and even conversion of IC engine powered vehicles into EVs. In this context the Electrical Mobility Laboratory (EMoL) was created at the IFSC. Reports on battery degradation and fire, along with the appreciation of the efforts of big car manufacturers towards battery thermal management, turned the attention of the EMoL team to the battery cell thermal behavior. It is a relatively recent concern for the team, as their first prototypes had cells exposed to the environment air that readily kept the temperatures under proper limits. The prospect of putting these cells in a sealed battery pack and offering it as part of a conversion kit (to be used at more challenging environmental conditions and power demands) triggered this initial study of battery cells thermal behavior. This study aims to support a more comprehensive electrothermal model discussed in a companion paper. The initial study reported here deals with basic heat transfer, initially in a single prismatic cell, using an analytical solution of three dimensional heat conduction to discuss the practical application of lumped capacitance analysis in some circumstances. The orthotropic properties used to model the multilayered cells as a single continuous medium brought the necessity of adapting the effective heat transfer coefficient calculation (used to extend lumped capacitance analysis applicability) to orthotropic media (something not existent in the literature, to the best of authors' knowledge). A coarse grid CFD solution is used for some qualitative analysis and a quick discussion of simple heat transfer models for a battery of cells cooled by air and by conduction is made, highlighting the first mistakes likely to occur in such studies and lessons already learned.*

Keywords: *Battery cell, Lumped analysis, Orthotropic conduction*

1. INTRODUCTION

An initial study of EV battery cells thermal behavior involves knowledge of some basic constructive aspects of the most common cell types and the demands that these cells are designed to meet. Nowadays there are many sites at the Internet helpful in the journey from that electrochemistry usually learnt in secondary school to a reasonable acquaintance with the kind of carbon-NMC Li-ion that is the subject of the present work. A very helpful source of information about this kind of cell, shaped at the prismatic geometry to be discussed here, directed to those interested in mathematical modeling, is the paper by Kleiner *et al.* (2020).

Carbon-NMC and carbon-$LiFePO_4$ are the two battery cell types most used in EV today. Based on an electrolyte consisting of $LiPF_6$ diluted in an organic liquid, they have a chemistry slightly different from the Li-polymer cells used in mobile phones, tablets and laptop computers and quite distinct from the Ni-MH cells used in the first hybrid vehicles widely available (Toyota Prius and Ford Fusion Hybrid, for instance).

Two rather visual aspects of EV Li-ion battery cells will be important to parts of the present study: (1) the three basic geometries (cylindrical, pouch and prismatic) in which they are manufactured and (2) the laminated internal structure that results from the disposition of alternate sheets of cathode, of polymer (porous PP or PE) separator soaked with electrolyte and of (typically carbon) anode. The laminated structure will determine an orthotropic behavior of the heat conduction inside the cells. The design option for one specific cell geometry reflects the priorities given to different goals: pouches are less expensive, small cylinders are amenable to temperature control and prismatic cells accommodate higher energy densities.

The most critical operation phase of a battery is usually its charging. At high environment temperatures (40 ºC) the heat generated by fast charging may be difficult to dissipate (but the battery internal resistance is lower) and at low temperatures (0 ºC) the tendency to lithium dendrites formation (and internal short circuit creation) while charging is increased. In fact the sophistication of the battery thermal management systems (BTMs) adopted by different car brands seems to reflect their approach to the fast battery charge challenge: those aiming the higher end of the EV car prices spectrum (like Tesla, Audi and Mercedes), offer super fast charging (at 250 kW) and adopt cylindrical cells cooled (and eventually heated) by liquid (actively refrigerated using the same compressor and condenser of the air conditioning, when necessary) circulating through aluminum piping around the cells. Those trying to make less expensive cars offer an also fast charge (notably VW in its MEB platform at 150 kW and not so impressively Chevrolet Bolt at 55 kW) with pouch or prismatic cells yet cooled actively by liquid circulation (inside a cold plate at the battery bottom). Finally some entry level models, like Renault Zoe and Nissan Leaf offer 55 kW fast DC charging for batteries passively cooled essentially by the air flowing around its casing (but it should be noticed that the actual charging speed attainable will depend strongly on the environment temperature for these models).

It is worth mentioning that early hybrid cars had their Ni-MH batteries cooled by the conditioned air from the vehicle interior. Maybe to avoid the health risks for passengers represented by gasses accidentally emitted by defective Li-ion batteries, new hybrids equipped with this type of battery (like the Mitsubishi Outlander PHEV) have different battery cooling systems (in the case of the Outlander the battery enclosure has its own evaporator and fan to circulate the air confined there). The fully electric BMW i3 has a cold plate under its battery, where the AC refrigeration fluid circulates (the plate is an evaporator) and in this aspect resembles the Outlander PHEV (both can be charged at 50 kW DC).

Without the ambition of offering super fast charging (no more than 22 kW DC charging) for former IC engine powered vehicles converted into EVs, prismatic cells were the primary choice in the project to which the present work belongs. Initial tests performed in a Fiat Fiorino converted to electric with a prototype kit involved continuous charges limited to 7 kW AC (although regenerative braking topped higher currents), a typical current of 30 A at 60 km/h, variations between 35 and 40 A at 80 km/h, but peaks of even 350 A (for a few seconds) and no significant temperature rise in the battery was observed. A more systematic study of the thermal behavior of the batteries developed in the project, and the assessment of the need for a simpler or more sophisticated temperature control system was still pending, however, and started as it is shown in the following sections.

2. STEADY STATE

Theoretical investigation of the steady state of the system is a good first step. For the cells under investigation, steady state temperatures above that of the environment are likely to occur only in the intermediate phase of a not too fast charge process (during discharges and most other operations the current experiences significant variations in time scales much smaller than these cells thermal time constants). The charge of the cells under investigation will be limited to "C/2" current intensity (this means, for a 113 Ah cell, 56.5 A, and considering the declared maximum internal resistance of 0,6 mΩ, a heat dissipation $q = 1{,}9$ W at each cell). Since the project requirements do not seem to justify the cost of a cooling liquid circulation circuit two alternatives will be considered: cooling by air circulation inside the battery compartment and cooling by heat conduction.

2.1 Cell cooled by air circulation

In this first analysis, it is assumed that each cell can be cooled uniformly by convection, ensued through the creation of an air circulation pattern with multiple symmetries to take the heat from the cells, represented by the orange rectangles to the cooler battery package external walls, represented, in Fig. 1 by the blue rectangles .

Assuming that the temperatures of the cells T_c and those of the external walls T_w are uniform, this situation can be described by models for heat exchangers with zero heat capacity ratio (Roetzel *et al.*, 2019). The space between the cells (gap) would be a relatively usual heat exchanger, with the temperature of the fluid stream of greater thermal capacity being tht of the cell. However, the space between the cells and the external wall surface (plenum), would be an exchanger with walls at different temperatures, which in a simplified one-dimensional model behaves like an exchanger with walls at an average temperature (weighted by the fin effectiveness, ϵ_w of the surface of the external wall, that may have some relief) of the temperature of the cell and that of the external wall.

The heat rate that leaves each (half of) cell $q/2$ would be the sum of what it loses to the usual exchanger in the q_{clgap}

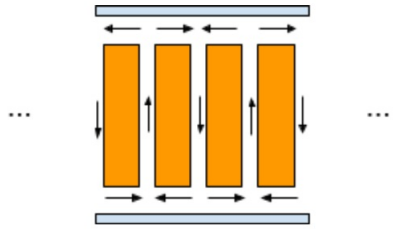

Figure 1. Repetitive pattern of air circulation around the cells

gaps with what it loses to the plenums $q_{\text{c|plenum}}$, while the heat received by the external walls consists only of what they receive from the plenums $q_{\text{w|plenum}}$ (and this heat rate must be equal, in each symmetrical secti on of the cell battery, to the heat lost by the cell above/below that section external walls). Calling the lower left corner of the first cell (of the four shown in the figure) point 0 and point 1 the lower right corner, and again point 0 the upper right corner (since it must have the same conditions as the starting point, only with the direction of the velocity reversed), the following equation system can be written.

$$\begin{cases} q_{\text{c|gap}} = \varepsilon_{\text{gap}} \dot{m} c_p (T_c - T_1) \\ q_{\text{c|plenum}} - q_{\text{w|plenum}} = \varepsilon_{\text{plenum}} \dot{m} c_p \left(\dfrac{T_c + \epsilon_w T_w}{1 + \epsilon_w} - T_0 \right) \\ q/2 = q_{\text{w|plenum}} = q_{\text{c|gap}} + q_{\text{c|plenum}} \\ q_{\text{c|gap}} = \dot{m} c_p (T_0 - T_1) \\ q_{\text{w|plenum}} = h_{\text{plenum}} \epsilon_w A_b \left\{ \dfrac{(T_0 - T_w) - (T_1 - T_w)}{\ln[(T_0 - T_w)/(T_1 - T_w)]} \right\} \end{cases} \tag{1}$$

where, besides the already mentioned fin effectiveness, the following heat exchanger effectiveness are also used

$$\varepsilon_{\text{gap}} = 1 - \exp\left(\frac{h_{\text{gap}} A_{\text{face}}}{\dot{m} c_p} \right) \qquad \varepsilon_{\text{plenum}} = 1 - \exp\left[\frac{h_{\text{plenum}} (1 + \epsilon_w) A_b}{\dot{m} c_p} \right] \tag{2}$$

In the equations above $\dot{m}$ is the mass flux (in kg/s) of air circulating around each cell, c_p is the air specific heat and h is the coefficient of heat transfer by convection, different in the plenuns and the gaps. The cells have theis surface diveded in A_{face}, exposed to the gaps, and A_b exposed to the plenum.

This non linear system of equations was solved using a robust software (Klein and Alvarado, 2002) but becomes very ill-conditioned when including the equations from the thermophysical properties library. To alleviate this difficulty the air properties were evaluated at the prescribed external wall temperature, T_w. The Fig. 2 below shows typical results obtained. These results were for an external wall temperature T_w = 40 ºC, 3 mm of gap between cells, 25 mm of plenum

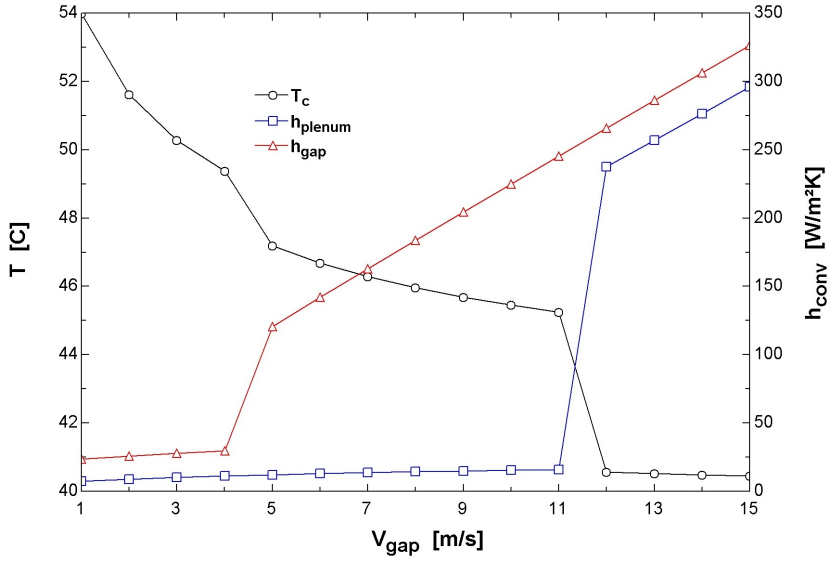

Figure 2. Cell temperature and convection heat transfer coefficients variation as air velocity increases

height and the cell dimensions that will bem detailed at the Tab. 1. It is possible to observe the transition to the turbulent flow regime in the gap between cells above 4 m/s and in the plenum just above 11 m/s causing a sudden increase in the convection heat transfer coefficients. To calculate the convection coefficient of heat transfer were used, in laminar flow, the Edwards et al. and in turbulent flow the Gnielinski correlation, respectively equations 8-64 and 8-70 in the book of Çengel and Ghajar (2011).

2.2 Cell cooled by conduction through an elastomer

In this second situation, one-dimensional conduction through the cell itself and an elastomeric medium that is interposed between its bottom and a single external wall can be considered.

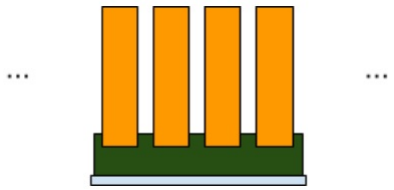

Figure 3. Cells over an elastomeric layer (green)

The generation of heat in the cells, which is mainly due to the Joule effect, is concentrated near the power connection terminals and to take this into account, the distribution given (in W/m³) by

$$q'''(x) = \frac{q}{LA_b}\left[\cos\left(\frac{\pi x}{L}\right) + 1\right] \tag{3}$$

At the bottom of the cell, the heat exchange with the external wall through the elastomer can be represented as a convection boundary condition (Robin condition in the context of differential equations) and next to the terminals, heat losses can be neglected (Neumann condition), obtaining the boundary value problem

$$\begin{cases} k\dfrac{\mathrm{d}^2T(x)}{\mathrm{d}x^2} + q'''(x) = 0 \\ \left.\dfrac{\mathrm{d}T}{\mathrm{d}x}\right|_{x=0} = 0 \qquad\qquad \left.\left(T + \dfrac{k}{h}\dfrac{\mathrm{d}T}{\mathrm{d}x}\right)\right|_{x=L} = T_w \end{cases} \tag{4}$$

where h is the ratio between the conductivity of the elastomer and the thickness of the layer that separates the cell from the battery package wall (floor). Its solution is

$$T(x) - T_w = \frac{q}{kLA_b}\left\{\frac{kL}{h} + \left(\frac{L}{\pi}\right)^2\left[1 + \cos\left(\frac{\pi x}{L}\right)\right] + \frac{L^2}{2}\left[1 - \left(\frac{x}{L}\right)^2\right]\right\} \tag{5}$$

Using the apparent thermal conductivity of the cell of 32 W/(m.K), suggested in paper of Wang *et al.* (2021) and the elastomer conductivity of 2 W/(m².K) for Bluesil ESA gap filler (Elkem Silicones, 2021), supposing a 0,025 mm thick elastomer layer, one gets a temperature rise (difference above the wall temperature) that does not reach 4 K (and the temperature variation across the cell is less than 19 % of the temperature variation across the elastomeric layer).

2.3 Order of magnitude analysis using Ohm's Law analogy

One can roughly represent both the use of confined air in a battery pack and the use of conduction through an elastomer (to carry heat from the cells to the battery enclosing walls) using analogue electrical circuits, as shown in the Fig 4.

In the analysis of the circuit depicted in the Fig 4, the temperatures T_{plenum} and the T_{gap} are not well defined (in fact, the average temperatures of the air in the plenum and in the gap would be the same, but in the plenum the local air temperatures are decreasing streamwise and in the gap increasing), the intention here is to emphasize that there is a temperature gradient through the air and that this (combined with the air movement) causes heat transport from the gap to the plenum. Likewise, the resistance $R_{\text{bottom|top}}$ of the cell in the (b) circuit does not have an exact expression, since the heat rate (analogous to electric current) does not originate at the top but is generated by the Joule effect along the cell. Analyzing the circuit (a), which represents transport by convection, although

$$R_{\text{c|plenum}} = \frac{1}{h_{\text{plenum}}A_b} \gtrsim R_{\text{w|plenum}} = \frac{1}{h_{\text{plenum}}\epsilon_w A_b} \tag{6}$$

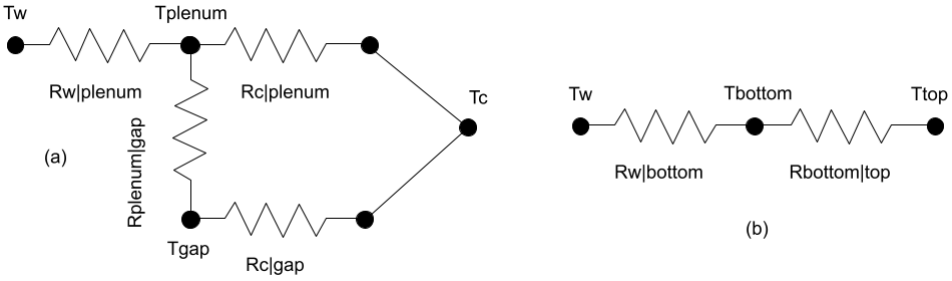

Figure 4. Circuits analogue to: (a) air circulation and (b) conduction through elastomer

it is reasonable to assume that

$$R_{\text{plenum|gap}} + R_{\text{c|gap}} = \frac{1}{\dot{m}c_p} + \frac{1}{h_{\text{gap}}A_{\text{face}}} \ll R_{\text{w|plenum}} = \frac{1}{h_{\text{plenum}}\epsilon_w A_b}$$
$$\therefore \qquad R_{\text{total}} \sim R_{\text{w|plenum}} = \frac{1}{h_{\text{plenum}}\epsilon_w A_b} \tag{7}$$

For the circuit (b) representative of heat transport by conduction through elastomer

$$R_{\text{w|bottom}} = \frac{L_{\text{elastomer}}}{k_{\text{elastomer}}A_b} \gtrsim R_{\text{bottom|top}} \approx \frac{L_y}{k_y A_b}$$
$$\therefore \qquad R_{\text{total}} \sim R_{\text{w|bottom}} = \frac{L_{\text{elastomer}}}{k_{\text{elastomer}}A_b} \tag{8}$$

where k_y and $k_{\text{elastomer}}$ are the thermal conductivities of the cell (in the vertical direction) and of elastomer, L_y and $L_{\text{elastomer}}$ are the height of the cell and the thickness of the elastomer layer.

3. TRANSIENT

The most representative transient behavior of the battery, when it responds to the dynamics of the vehicle under a realistic travel schedule, is discussed elsewhere (Gonçalves *et al.*, 2022). In this section preparatory studies of a single cell behavior in a very simple experiment of cooling from an initial uniform temperature by natural convection is addressed. This study was used not only to assess the battery cell thermal behavior but also the tools available to investigate and simulate this.

The first point to be made clear is that there was an actual experiment in which a cell (protected by a plastic film) was initially warmed in tepid water for several minutes and then was hanged by tiny strings at a room without wind currents and its surface temperature was monitored using some thermistors placed at different faces of the prismatic cell (trapped between the cell and the plastic film used to protect it from water). So the models to be presented in this section were built to be compared with the experimental results, as will be made at the end of the present work (in a single summarizing graph, so the models will be presented first, starting from the simplest).

3.1 Lumped capacitance model

The measurements obtained in the experiment revealed that the thermistors temperatures initially departed from the exponential behaviour expected from the mean temperature of the cell. This certainly occurred partially because of a difference between the thermistor and the cell surface temperatures and partially because of the differences between the temperatures at the cell surface and the cell mean temperature (differences that limit the applicability of the lumped capacitance analysis). It is reasonable to assume that at least the thermistor may be analyzed by the lumped capacitance method and so its temperature T_t may be related to the temperature of the surrounding air T_∞ and with the cell mean temperature T_c by

$$M_t c_{p_t} \frac{\mathrm{d}T_t}{\mathrm{d}t} = \frac{T_c - T_t}{R_{ct}} - \frac{T_t - T_\infty}{R_{t\infty}} \tag{9}$$

where M is used for the component mass, R for thermal resistance and the subscripts follow the logic used for the temperatures. The mean cell temperature T_c itself will be calculated using a slightly "extended" lumped capacitance method, using an effective heat transfer coefficient h_{ef} that will receive more attention later

$$M_c c_{p_c} \frac{\mathrm{d}T_c}{\mathrm{d}t} = -h_{\text{ef}} A_c (T_c - T_\infty) \tag{10}$$

For the above equation it is well known the classical solution

$$\frac{T_c - T_\infty}{T_0 - T_\infty} = \exp\left(-\frac{h_{\text{ef}} A_c}{M_c c_{p_c}} t\right) \tag{11}$$

and substituting this in (9) one gets

$$M_t c_{p_t} \frac{\mathrm{d}T_t}{\mathrm{d}t} = \frac{T_0 - T_\infty}{R_{ct}} \exp\left(-\frac{h_{\text{ef}} A_c}{M_c c_{p_c}} t\right) - \left(\frac{1}{R_{ct}} + \frac{1}{R_{t\infty}}\right)(T_t - T_\infty) \tag{12}$$

that itself has an analytical solution (easily obtained, with the help of symbolic algebra software)

$$\begin{aligned} \frac{T_t - T_\infty}{T_0 - T_\infty} = &\left[1 - \left(1 + \frac{R_{ct}}{R_{t\infty}} - \frac{h_{\text{ef}} A_c R_{ct} M_t c_{p_t}}{M_c c_{p_c}}\right)^{-1}\right] \exp\left(-\frac{R_{ct} + R_{t\infty}}{R_{ct} R_{t\infty} M_t c_{p_t}} t\right) \\ &+ \left(1 + \frac{R_{ct}}{R_{t\infty}} - \frac{h_{\text{ef}} A_c R_{ct} M_t c_{p_t}}{M_c c_{p_c}}\right)^{-1} \exp\left(-\frac{h_{\text{ef}} A_c}{M_c c_{p_c}} t\right) \end{aligned} \tag{13}$$

3.2 Three-dimensional heat conduction inside the cell analytical model

For uniform initial temperature, constant ambient temperature and thermal properties, a solution in the classical form of a series of orthogonal functions can be obtained, as explained in the chapter 2 of Öziçik (1993).

$$\begin{aligned} T(x,y,z,t) - T_\infty = &\sum_{p=1}^{\infty}\sum_{n=1}^{\infty}\sum_{m=1}^{\infty} c_{mnp} \exp\left[-\alpha(\beta_m^2 + \gamma_n^2 + \eta_p^2)\, t\right] \\ &\times \cos(\beta_m x) \cos(\gamma_n y) \cos(\eta_p z) \end{aligned} \tag{14}$$

where β_m, γ_n and eta_p are eigenvalues (calculated as explained in that same chapter). An invaluable hint is given, in the chapter 15 of this book of Öziçik (1993), to deal with orthotropic media as that in the interior of the cells. It consists in the use of the coordinates transformation described by the equations

$$X = x\sqrt{\frac{k}{k_x}} \qquad Y = y\sqrt{\frac{k}{k_y}} \qquad Z = z\sqrt{\frac{k}{k_z}} \tag{15}$$

The equivalent isotropic conductivity (to be used after the above coordinates transformation) can be calculated and then the thermal diffusivity to be used in the solution

$$k = \sqrt[3]{k_x k_y k_z} \qquad \alpha = k/(\rho\, c_{p_c}) \tag{16}$$

It is not usual really start using capital letters for the spatial coordinates (the transformed coordinates just assume the positions and the symbols formerly dedicated to the original ones), but in the remaining lines of this subsection it will be done to make contrast with the next subsection where the coordinates transformation will appear explicitly in the equations (not implicitly as a step that changes the exact meaning of some symbols as usual). The coefficients determined by the initial condition to the problem at hand are simply

$$c_{mnp} = (T_0 - T_\infty)\, \frac{\sin(\beta_m L_X) \sin(\gamma_n L_Y) \sin(\eta_p L_Z)}{\beta_m N(\beta_m)\, \gamma_n N(\gamma_n)\, \eta_p N(\eta_p)} \tag{17}$$

where $N(\beta_m)$, $N(\gamma_n)$ and $N(\eta_p)$ are respectively the the norms of the eigenfunctions $\cos(\beta_m X)$, $\cos(\gamma_n Y)$ and $\cos(\eta_p Z)$.

3.3 Extended lumped capacitance model

In order to extend the validity of the lumped capacitance method to situations where the Biot number $Bi = hL/k$ is not smaller then 0,1, Ranmod *et al.* (2019) provide, in table 1 of their article, an expression for an effective heat transfer coefficient h_{ef} that, for a cuboid geometry, takes into account the thermal internal resistence inside the solid. In the analysis performed by those authors, however, the material is considered isotropic and some adaptation is needed to deal with the orthotropy of the EV battery cells material. This can be accomplished using the approach explained in the previous subsection.

The expression of the effective heat transfer coefficient becomes simpler if dimensional eigenvalues are used instead of the dimensionless ones used by Ranmod *et al.* (2019). The dimensional first eigenvalues are the smallest positive roots of the equations

$$\beta_1 \tan\left(\beta_1 L_x \sqrt{\frac{k}{k_x}}\right) = \frac{h}{k} \qquad \gamma_1 \tan\left(\gamma_1 L_y \sqrt{\frac{k}{k_y}}\right) = \frac{h}{k} \qquad \eta_1 \tan\left(\eta_1 L_z \sqrt{\frac{k}{k_z}}\right) = \frac{h}{k} \tag{18}$$

and then

$$h_{\text{ef}} = k\,\frac{(\beta_1^2\,\gamma_1^2\,\eta_1^2)\,L_xL_yL_z}{L_xL_y + L_yL_z + L_xL_z} \tag{19}$$

The definition of k is the same given by Eq. (16) but all the lengths are the original ones, the adaptations to deal with the orthotropy were made directly in the Eqs. (18).

3.4 CFD model

The computational fluid dynamics resources offered by the SolidWorks Flow Simulation Add-in were explored in an attempt to obtain qualitative results and identify discrepancies with the previously presented three-dimensional analytical model. A presentation of the theoretical basis of the Add-in is found in Sobachkin and Dumnov (2013).

As no detailed information about the interior of the cell was available, it was considered a cuboid of an orthotropic solid here as it was in the three-dimensional analytical solution. The difference arises essentially in the boundary conditions for the solid that are no longer based on a uniform heat transfer coefficient. The cooling by natural convection modeled with CFD using a relatively coarse grid (as the results pursued were of qualitative nature) reproduces a vertically asymmetric pattern of heat transfer that is dismissed in the analytical model.

3.5 Numerical data and results

Some properties of the cells, the environment and also of the thermistors must be known to enable someone to obtain numerical results. The following tables summarize the most important properties values used. The specific heat of the

Table 1. Basic data of L221N113A cell offered by Zaozhuang Evlithium Electronic Technology Co. Ltd.

Property	symbol	unit	value
half width	L_x	m	$110{,}4 \times 10^{-3}$
half height	L_y	m	$52{,}94 \times 10^{-3}$
half thickness	L_z	m	$16{,}68 \times 10^{-3}$
mass of an eighth of a cell	M_c	kg	$0{,}225$

Table 2. Orthotropic thermal conductivity of the "jelly roll" (rolled and flattened sheets of electrical insulation, electrodes and spacer soaked with electrolyte) according to Kleiner *et al.* (2020)

Direction	symbol	unit	value
in plane (x and y)	k_x and k_y	W/(m·K)	33
across the thickenss (z)	k_z	W/(m·K)	0,7

Table 3. Properties attributed to a thermistor

Property	symbol	unit	value
mass	M_t	kg	$7{,}5 \times 10^{-5}$
specific heat	c_{p_t}	kJ/(kg·K)	$0{,}45$
surface area	A_t	m²	$3{,}2 \times 10^{-5}$

cell was experimentally evaluated by the authors as $c_{p_c} = 0{,}93$ kJ/(kg·K). From the data in Tab. 1 the cell density is calculated as $\rho = 2{,}3 \times 10^3$ kg/m³. In the experiment (and also in the theoretical results to be compared with it) the initial temperature of the cell was $T_0 = 57$ ºC and the air temperature $T_\infty = 23$ ºC.

The Figure 5 summarizes the measurements and theoretical results for the transient problem at hand. The measurements are represented by the first 5 entries in the legend of Fig. 5 and by the curves that exhibit lower temperatures in the graph (only the lumped capacitance analysis result for the thermistor temperature was really able to reproduce these measurements). These measurements are identified with different positions at the cell surface where the thermistors that produced them were placed (the + and - conectors are at the top of the cell).The extended lumped capacitance results are represented by the 6th and 7th entries in this legend and correspond to the mean cell temperature and to the temperature of a thermistor placed at the cell surface (considered approximately isothermal). The 8th and 9th entries in the same legend represent the minimal and maximal temperatures in the cell calculated using the coefficient of heat transfer by convection

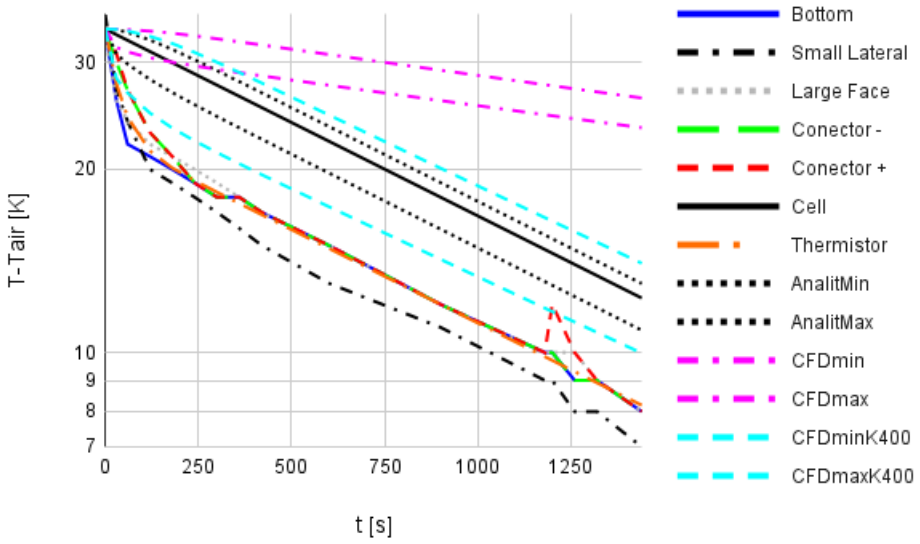

Figure 5. Summary of measurements (first 5 legend entries) and theoretical results

$h = 22{,}5$ W/(m²·K) and ten eigenfunctions for each direction in the summations at Eq. (14). The Figure 6 depicts the temperature field yielded by this analytical model for $t = 900$ s after the start of the cell cooling.

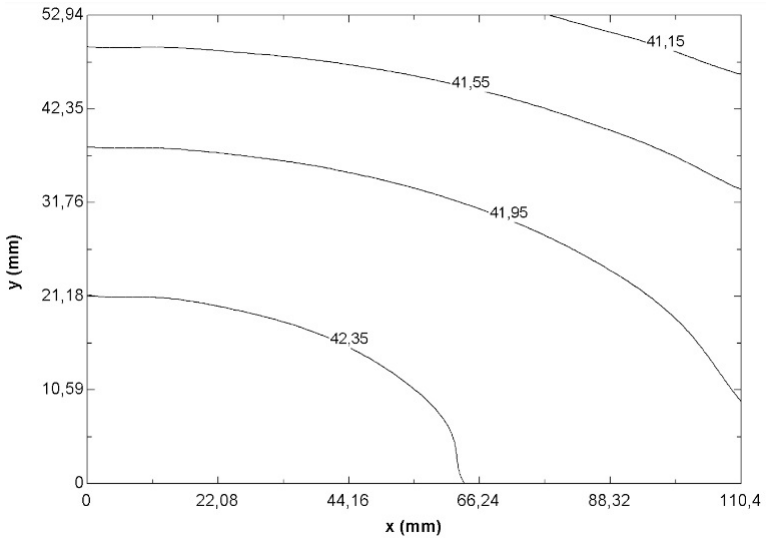

Figure 6. Analytically obtained isotherms (labels are in ºC) at the top right quarter of the larger cell face (plane $x \times y$)

The 10th and 11th entries in the legend of Fig. 5 represent results obtained using the default far field boundary conditions for the natural convection problem in the Solid Works Flow Simulation Add-in. A temperature map to be compared to that shown in Fig. 6 was prepared using this CFD model and is presented in the Fig. 7. Since these first CFD results presented a behavior markedly different of that observed in the experiment (essentially the average heat transfer coefficient obtained was too low) it was attempted to increase the turbulent kinetic energy $kappa$ at the far field boundary, to enhance the heat transfer. So the 12th and 13 thentries in the legend of Fig. 5 represent CFD results obtained using $\kappa = 400$ J/m³ at the far field boundary. Again a temperature map to be compared to those shown in Fig. 6 and Fig. 7 was prepared and is presented in the Fig. 8. These last CFD results reveal a much better agreement with the analytical results and the measurements, but the level of turbulence attributed to the far field boundary condition is typical of a high power fan exit and is much higher than anything possible to find in the environment where the experiment was developed. So the CFD models assembled in this study deserve improvement, but CFD modeling is not priority in this project by now.

It is important to make clear that the CFD model did not provided worse predictions than the lumped capacitance or the analytical models. What really happened is that in these latter models the convection heat transfer coefficient was used as a fitting parameter to match the experimental data. A CFD software calculates the convection heat transfer in the air according to grid and boundary conditions much more difficult to tune. By the way, using the $h_{ef} = 17{,}1$ W/(m²·K)

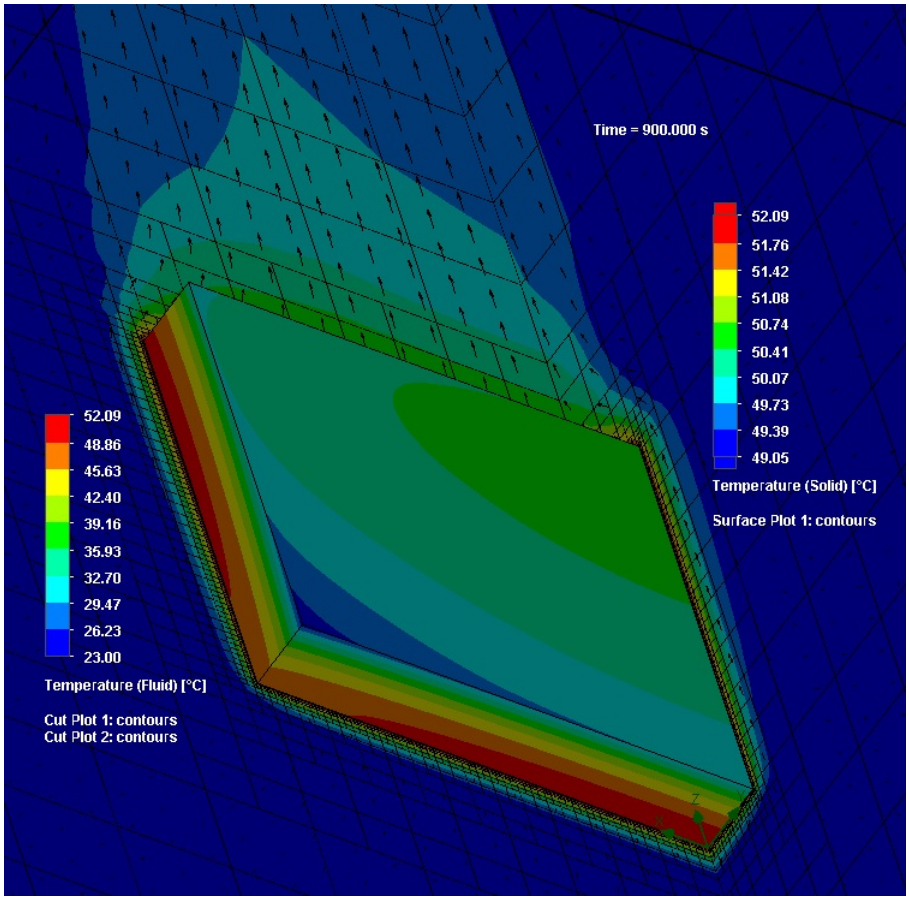

Figure 7. CFD results around the front left quarter of the cell (default boundary conditions)

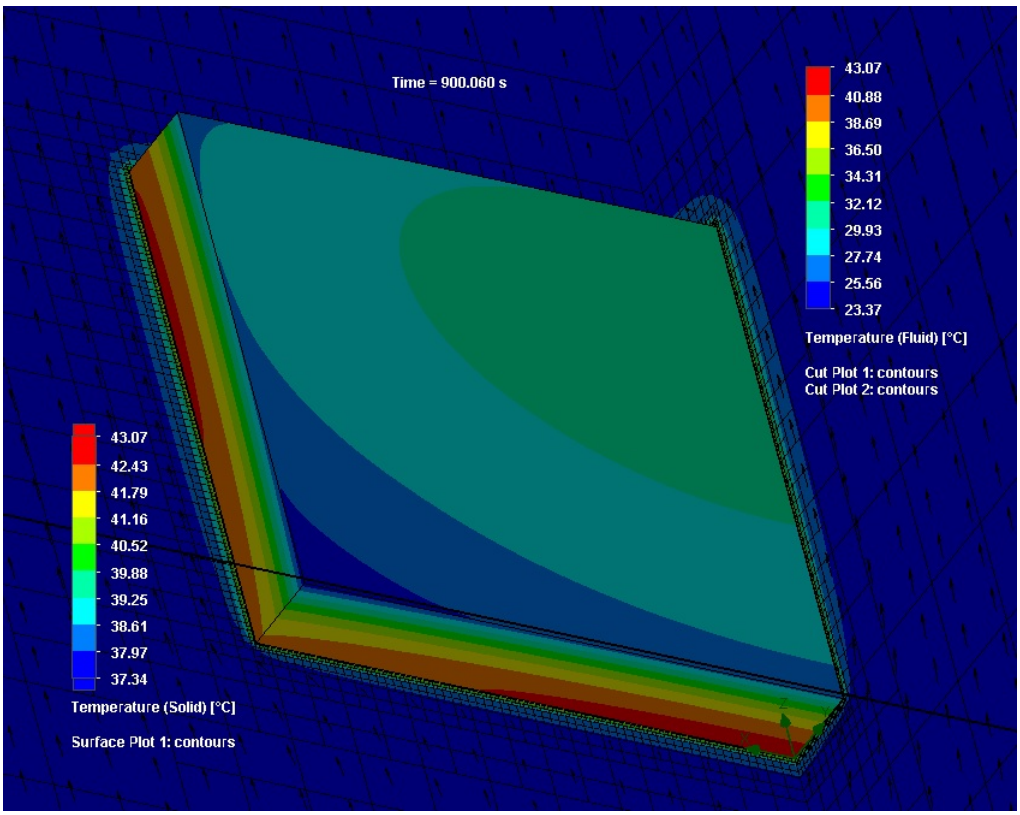

Figure 8. CFD results around the front left quarter of the cell with $\kappa = 400$ J/m³ at boundaries

obtained from the inclination of the experimental curves in Fig. 5 and solving a system of nonlinear equations formed by Eqs. (18) and (19) the value of $h = 22{,}3$ W/(m²·K) was found.

4. CONCLUSION

A variety of modeling tools were explored in this work, from a simplistic heat exchanger network operating in steady state, to analytical heat conduction models for steady state and transient regimes and finally CFD (without dismiss a crude but clarifying order of magnitude analysis). This exploration is helpful in order to choose those to be used in further studie of EV batttery thermal behavior.

This initial study was not expected to yield design guidelines for an EV battery thermal management system. It was rather intended to provide insight in some phenomena involved in these systems, reveal some difficulties likely to be found during the building of more sophisticated transient models (to deal with the time varying heat generation inside the battery) and also care to be taken when comparing theoretically predicted temperatures with measurements. These goals were reached and in this sense, as in the sense of being pleasant to make, this work was really satisfactory.

5. ACKNOWLEDGEMENTS

The authors acknowledge the financial support from ANEEL, CELESC, EMBRAPII and IFSC. The authors are thankful for the collaboration of many colleagues and students, specially that of Mr. João Pereira Pacheco and Mr. João Vitor Calazans.

6. REFERENCES

Elkem Silicones, 2021. "Battery thermal management in hybrid & electric vehicles: Silicone solutions for efficient insulation or conduction". Ebook. URL https://content.elkem.com/eBook-Battery-Thermal-Management.

Gonçalves, J.M., Abreu, S.L., Santos, L.A., Bresolin, A.A., Fuerback, A.L. and Costa, D.G., 2022. "Electrothermal simulation of electric vehicle battery under driving conditions". paper submitted to ENCIT 2022.

Klein, S. and Alvarado, F., 2002. "EES-engineering equation solver". F-chart software. URL https://fchartsoftware.com/ees/.

Kleiner, J., Komsiyscka, L., Elger, G. and Endisch, C., 2020. "Thermal modelling of a prismatic lithium-ion cell in a battery electric vehicle environment: Influences of the experimental validation setup". *Energies*, Vol. 13, No. 1. URL https://www.mdpi.com/1996-1073/13/1/62.

Ranmod, V., Singh, M. and Bhattacharya, J., 2019. "Analytical formulation of effective heat transfer coefficient and extension of lumped capacitance method to simplify the analysis of packed bed storage systems". *Solar Energy*, Vol. 183, pp. 606–618. URL https://www.sciencedirect.com/science/article/pii/S0038092X19302956.

Roetzel, W., Luo, X. and Chen, D., 2019. *Design and Operation of Heat Exchangers and their Networks*. Academic Press, 1st edition.

Sobachkin, A. and Dumnov, G., 2013. "Numerical basis of CAD-embedded CFD". NAFEMS World Congress. URL https://www.solidworks.com/sw/docs/flow_basis_of_cad_embedded_cfd_whitepaper.pdf.

Wang, N., Li, C., Li, W., Huang, M. and Qi, D., 2021. "Effect analysis on performance enhancement of a novel air cooling battery thermal management system with spoilers". *Applied Thermal Engineering*, Vol. 192, p. 116932. URL https://www.sciencedirect.com/science/article/pii/S1359431121003793.

Çengel, Y. and Ghajar, A., 2011. *Heat and Mass Transfer*. McGraw-Hill Education, 4th edition.

Öziçik, M.N., 1993. *Heat Conduction*. Wiley-Interscience, 2nd edition.

7. RESPONSIBILITY NOTICE

The authors are solely responsible for the printed material included in this paper.